

國立臺灣大學電機資訊學院資訊工程學研究所



碩士論文

Department of Computer Science and Information Engineering

College of Electrical Engineering and Computer Science

National Taiwan University

Master Thesis

基於同時調整多策略以最佳化零力矩點軌跡

實現人型機器人之行走平衡

Future ZMP Trajectory Optimization with Simultaneous  
Multi-Strategy Adjustment for Humanoid Walking Balance

王邦丞

Bang-Cheng Wang

指導教授：王傑智 博士

Advisor: Chieh-Chih Wang, Ph.D.

中華民國 一百零四 年 一 月

January, 2015

國立臺灣大學碩士學位論文  
口試委員會審定書

基於同時調整多策略以最佳化零力矩點軌跡實現人型  
機器人之行走平衡

Future ZMP Trajectory Optimization with Simultaneous  
Multi-Strategy Adjustment for Humanoid Walking Balance

本論文係王邦丞君（學號 R02922166）在國立臺灣大學資訊工程  
學系完成之碩士學位論文，於民國 103 年 12 月 24 日承下列考試  
委員審查通過及口試及格，特此證明

口試委員：

王傑智

（指導教授）

宋開泰

郭振華

柯沛群

趙坤茂

系主任

## 誌謝

在此論文完成之際，首先要感謝我的指導教授王傑智老師對我的諄諄教誨、教導我研究方法、培養我研究的能力、讓我了解什麼是正確的研究態度。其次感謝諸位實驗室學長在我每當研究遇到瓶頸時及時為我解惑，引導我走向研究道路。感謝實驗室諸位同學學弟們能陪伴我在漫長的研究生生涯裡苦中作樂。感謝親戚們在我台北念書時總是視如己出照顧我。最後感謝我的家人總是無怨無悔的支持我，讓我能無憂無慮專心做研究。這份論文是靠眾多貴人相助才得以完成，絕非憑一己之力可及，在此對各位獻上誠摯的感謝。



## 中文摘要

人形機器人走路時一件富有挑戰性的控制問題。現今研究已發現可以基於調整控制輸入、步伐大小和步伐長度三種策略的未來零力矩點(Zero-Moment Point)軌跡來增進機器人平衡。然而，我們發現現今方法由於未考慮多策略之間的相互關係，因此增進平衡的能力是受限制的。在此論文中，我們分析多策略之間的相互關係，並且提出基於同時調整多策略以最佳化零力矩點軌跡實現人型機器人之行走平衡，而最佳化未來零力矩點軌跡是透過最佳化能量函數所產生的。最後，本研究與現今頂尖的零力矩點軌跡調整方法比較，並證明此演算法能夠讓機器人在更艱難條件下維持平衡。





# FUTURE ZMP TRAJECTORY OPTIMIZATION WITH SIMULTANEOUS MULTI-STRATEGY ADJUSTMENT FOR HUMANOID WALKING BALANCE

**Bang-Cheng Wang**

Department of Computer Science and Information Engineering  
National Taiwan University  
Taipei, Taiwan

January 2015

*Submitted in partial fulfilment of  
the requirements for the degree of  
Master of Science*

**Advisor: Chieh-Chih Wang**

Thesis Committee:  
Kai-Tai Song  
Jen-Hwa Guo  
Pei-Chun Lin

© BANG-CHENG WANG, 2015



## ABSTRACT

---

**H**UMANOID walking balance has been a challenging issue in the control field since the balance can only be achieved by considering the dynamics of the system. It is found that the modification of the future ZMP trajectory based on the multiple strategies, which are the adjustment of the control input, the step size and the step duration, can enhance the robot balance. However, the capacity of the disturbance compensation is limited due to the fact that the correlation among the strategies is not considered. In this work, the correlation among the three strategies is analyzed, and the future ZMP trajectory optimization with simultaneous multi-strategy adjustment for humanoid walking balance is proposed. After defining an energy function for the robot balance, an optimized trajectory based on the simultaneous adjustment is generated. By comparing our work with the state-of-the-art future ZMP trajectory modification approaches, it is shown that our approach can maintain the robot balance under more severe situations.



## TABLE OF CONTENTS

---

ABSTRACT . . . . .	ii
LIST OF FIGURES . . . . .	iv
LIST OF TABLES . . . . .	v
CHAPTER 1. Introduction . . . . .	1
CHAPTER 2. Related Work . . . . .	4
CHAPTER 3. Foundation . . . . .	7
3.1. Optimal Control based on Linear Inverted Pendulum Mode . . . . .	7
3.2. Non-divergent Condition . . . . .	11
3.3. Three Strategies for Maintaining Robot Balance . . . . .	13
CHAPTER 4. Trajectory Optimization with Simultaneous Multi-Strategy Adjustment	14
4.1. Correspondence between the Future ZMP Trajectory and the Three Strategies	14
4.2. Correlation among the Three Strategies . . . . .	16
4.3. Trajectory Optimization with Simultaneous Multi-Strategy Adjustment . . . .	20
4.4. Comparison with the Three-strategy-based and the Heuristic-strategy-based Approaches . . . . .	25
CHAPTER 5. Experiment Result . . . . .	28
5.1. Simulation Experiment . . . . .	28
5.1.1. Configuration of the Simulated Humanoid Robot . . . . .	28
5.1.2. Experiment with Various Cycles of Disturbance . . . . .	29
5.2. Real Environment Experiment . . . . .	33
CHAPTER 6. Conclusion and Future Work . . . . .	37
BIBLIOGRAPHY . . . . .	38



## LIST OF FIGURES

---

3.1	Example of the LIPM . . . . .	8
3.2	Preview Gain $G_d$ ( $\Delta t = 10$ ms, $z = 255$ mm, $Q_e = 1$ , $R = 10^{-10}$ ) . . . . .	10
3.3	Preview Gain $G_r$ ( $\Delta t = 10$ ms, $z = 255$ mm, $Q_e = 1$ , $R = 10^{-10}$ ) . . . . .	12
4.1	Correlation between $\Delta u(k+i)$ and $\Delta m_c$ ( $\Delta t = 10$ ms, $s_c = 25 \Delta t$ , $N_L = 200$ ) . . . . .	17
4.2	Correlation between $\Delta u(k+i)$ and $\Delta s_c$ ( $\Delta t = 10$ ms, $s_c = 25 \Delta t$ , $N_L = 200$ ) . . . . .	18
4.3	Correlation between $\Delta m_c$ and $\Delta s_c$ ( $\Delta t = 10$ ms, $s_c = 25 \Delta t$ , $N_L = 200$ ) . . . . .	19
4.4	Correlation among the Three Strategies . . . . .	20
4.5	Selection of $\alpha$ and $\beta$ . . . . .	22
4.6	Example of Our Approach and the Three-strategy-based Approach in the Sagittal Plane . . . . .	26
4.7	Example of Our Approach and the Heuristic-strategy-based Approach in the Lateral Plane . . . . .	26
5.1	ZMP Trajectory without Disturbance . . . . .	29
5.2	Our Approach with Single-Cycle Disturbance . . . . .	30
5.3	Nishiwaki and Kagami's Approach with Single-Cycle Disturbance . . . . .	30
5.4	Urata et al.'s Approach with Single-Cycle Disturbance . . . . .	30
5.5	Our Approach with Multiple-Cycle Disturbance . . . . .	32
5.6	Nishiwaki and Kagami's Approach with Multiple-Cycle Disturbance . . . . .	32
5.7	Urata et al.'s Approach with Multiple-Cycle Disturbance . . . . .	32
5.8	Multiple-Cycle Random Disturbance . . . . .	34
5.9	Real Environment Experiment Setting . . . . .	35
5.10	Sagittal Plane Experiment . . . . .	36
5.11	Lateral Plane Experiment . . . . .	36





## LIST OF TABLES

---

5.1 Comparison with Single-Cycle Disturbance . . . . .	29
5.2 Comparison with Multiple-Cycle Disturbance . . . . .	31
5.3 Comparison with Multiple-Cycle Random Disturbance . . . . .	33



## CHAPTER 1

---

### Introduction

**H**UMANOID robot walking balance has been a challenging problem. The challenging issues are described as follows: First, the degree of freedom (DoF) of the control space is high. In general, an omni-directional humanoid robot has 12 DoFs in its leg, for example, ASIMO (Hirai et al., 1998) and HPR-2 (Kaneko et al., 2004). Although some robots have less than 12 DoFs, such as Nao (Gouaillier et al., 2009), the DoFs is still high and makes the control problem difficult. Second, the balance of the humanoid robot can be only achieved by considering the robot dynamics. Since most of the time the robot is supported with one foot and its center of mass is outside the support polygon of the robot, the static balance of the robot cannot be acquired and the robot must consider its dynamics to maintain balance. Finally, in the real environment the disturbance occurs everywhere, such as inaccurate motor, uneven terrain and pushing from external force, and the robot needs to suppress the disturbance to remain balance. In this thesis, we focus on the third issue, which is the disturbance suppression of the robot.

The most popular criterion to stabilize the robot is based on the concept of the Zero-Moment Point (ZMP) (Kajita et al., 2006; Sugihara, 2009; Morisawa et al., 2010). The ZMP (Vukobratovic et al., 1970) is a concept in which the ground reaction force does not provide any moment in the horizontal plane. It is widely used in humanoid robot walking, since the robot can remain balance if and only if the ZMP is inside the support polygon. Since the ZMP has been introduced, the humanoid robot walking problem has been transferred into a control problem whose main objective is to keep the ZMP inside the support polygon. However, in the real robot, the control of the ZMP is hard to realize due to the complex

dynamics of the robot. Therefore, researchers simplify the control problem of the robot walking into an inverted pendulum problem, where the robot is assumed to be a point mass called Center of Mass (CoM). Kajita et al. (Kajita et al., 2001) introduced the idea of the 3D Linear Inverted Pendulum Mode (LIPM) and showed that given the constraint that the CoM moves on a plane, the dynamics of the CoM and ZMP can be linearized and the motion can be decomposed into sagittal plane and lateral plane. Furthermore, the LIPM is combined with the Optimal Control (Katayama et al., 1985) to provide an optimal control input given a future ZMP trajectory (Kajita et al., 2003).

Since the optimal control was introduced into the humanoid robot walking, researchers have found that the adjustment of the future ZMP trajectory can maintain the balance of the robot. The three strategies for changing the future ZMP trajectory, which are the change of the reference ZMP inside the sole during a step, the change of the current step duration and the change of the current step size, is proposed and applied sequentially to maintain the balance in humanoid walking (Nishiwaki & Kagami, 2010). In addition, a non-divergent condition (Urata et al., 2011) is introduced and shown that once the future ZMP trajectory satisfies the condition, the CoM trajectory will not diverge. Then, the condition is combined with the adjustment of the step size (Urata et al., 2011) to allow the robot to change its step position rapidly and suppress the disturbance. However, we found that the capability of the disturbance endurance in their works is relatively small when their works are applied in the Nao platform. We believe that the capability is limited because the correlation among the three strategies is not considered.

In this work, first we evaluate the correspondence between the future ZMP trajectory and the three strategies to show how the future ZMP trajectory is constructed with the three strategies. Next we analyze the correlation among the three strategies and show that the three strategies affect each other. In addition, we argue that the adjustment of the reference ZMP inside the sole during a step can be transferred into the adjustment of the control input; therefore, the three strategies in our work will be: the adjustment of the control input, the step size and the step duration of the current step. Then, we transfer the combination problem of the three strategies into an optimization problem whose target is to minimize an energy cost function which is composed of the control input and the modification of the current step size. Our approach is tested in both simulation and real environment to show the enhancement of the disturbance endurance.

The thesis is organized as follows. First we introduce the related works of the walking and balance of the humanoid robot in Chapter 2. In Chapter 3, the foundation of our work is explained in detail. In Chapter 4, the analysis of the correlation among the three strategies and the simultaneous application of the three strategies are proposed. In Chapter 5, both the simulation and the real environment experiments are demonstrated and explained in detail. Finally, we summarize and discuss our future work in Chapter 6.



## CHAPTER 2

---

### Related Work

**H**UMANOID robot walking has been a long term research. Since the concept of the ZMP has been introduced by Vukobratović et al. (Vukobratovic et al., 1970), researchers has been focusing on how to keep the ZMP inside the support polygon when the disturbance occurs. The concept of the Capture Point (CP) (Pratt et al., 2006; Engelsberger et al., 2011), which is a point on the ground where the robot can step to make itself a complete stop, was introduced and shown that with this point, the robot can recover balance after a push. Sugihara extended the idea of the CP and introduced the concept of the Best CoM-ZMP Regulator (Sugihara, 2009), in which the robot is in the standing-stabilizable condition if the state of the CoM satisfies the standing-stabilizable criteria. Kajita et al. proposed the auxiliary ZMP control to deal with the challenging environment such as outdoor uneven terrain (Kajita et al., 2006, 2010). In other approaches, the reactive stepping is also considered to suppress the disturbance. Morisawa et al. analyzed the foot contact on a terrain and proposed a reactive-stepping method to balance for different contact times (Morisawa et al., 2010, 2011). Santacruz and Nakamura proposed a reactive stepping strategy based on the Neutral Point and the Boundary Condition Optimization to compensate the disturbance (Santacruz & Nakamura, 2013). These approaches were tested on the human-size robot and shown to suppress the disturbance successfully.

In addition to human-sized robots, recently humanoid Nao robot (Gouaillier et al., 2009) has gained more attention when talking about robot balance owing to the requirement of the walking stableness when the robot is attending a competition, such as RoboCup Standard Platform League. Unlike human-sized robots, the Nao robot has limited capacity

of measuring the ZMP since the force sensor resistors are inaccurate. Therefore, the traditional balance approach cannot be applied for the Nao robot directly. The adjustment of the CoM trajectory based on the LIPM in real-time by observing the status of the CoM is proposed (Graf & Röfer, 2012) and the walking abilities of the robot with the approach is demonstrated in the RoboCup scenario. Czarnetzki et al. proposed an Observer-based Control for biped robot (Czarnetzki et al., 2009), which is based on optimal control, and showed that Nao can balance itself by this approach. Urbann and Hofmann (Urbann & Hofmann, 2014) argued that by modifying the future steps of the robot, the error between the reference and the system output from the optimal control can be minimized. Xue (Xue et al., 2012) proposed an Elasticity Modeling Control (EMC) to compensate the disturbance from the hip roll joint of the robot, and showed that the robot can achieve a higher walking speed with this approach. Alcaraz-Jimnez et al. argued that when the robot suffers a disturbance that generates an angular momentum, the robot tilts and the ZMP is at the limit of the support polygon, which may cause the robot oscillate around the rotation axis repeatedly (Alcaraz-Jiménez et al., 2013). Therefore, they proposed an angular momentum control, which consists of a P controller, to suppress the oscillation by observing the rotation of the torso and adding an increment CoM position to the current state.

Furthermore, researchers have found that the future ZMP trajectory can affect the stability of the robot. Nishiwaki and Kagami (Nishiwaki & Kagami, 2010) proposed a three-strategy-based approach by considering three strategies for changing the reference ZMP trajectory. The three strategies are the adjustment of the reference ZMP during the current step, the step duration and the step size of the current step. They showed that there exists analytical solution for the adjustment of the step duration and the step size, and the robot can be balanced by adjusting the future ZMP trajectory with the combination of the three strategies. Then, they (Nishiwaki & Kagami, 2011, 2012) introduced the Permissible Region (PR) to suppress the change of the ZMP by modifying the control input of the current step at the moment when the disturbance occurs. In addition, Urata et al. (Urata et al., 2011) showed that by setting a proper value of the tracking-error weight  $Q$  and the control input weight  $R$  in the optimal control ( $Q \gg R$ ), the output ZMP can track the reference ZMP. Given the assumption above, Urata et al. (Urata et al., 2012) proposed a heuristic-strategy-based approach that changes the future step size to compensate the disturbance. Both of their approaches were tested on a real robot and showed that the robot

can remain stable under the disturbance. However, in their works, the correlation among the strategies was not considered. In the traditional three-strategy-based approach, since only the strategy that adjusts the step size is applied in the sagittal plane, if the output step size exceed the robot limitation, the robot will fall down. Here we argue that by considering the correlation between the ZMP reference during the current step and the step size, the excessive step size can be reduced with the adjustment of the ZMP reference during the current step. In addition, in the heuristic-strategy-based approach, the step duration is not modified when there is a disturbance from the opposite side of the support foot of the robot, and this may result in the robot falling in the lateral plane when the output ZMP is outside the support polygon. In our approach, the step duration and the control input are adjusted simultaneously to keep the ZMP inside the support polygon.



## CHAPTER 3

---

### Foundation

**I**N Section 3.1, we will introduce the traditional idea of the **Linear Inverted Pendulum Mode (LIPM)** and the **Optimal Control** and show how they can be combined to generate the walking pattern. In Section 3.2, we will introduce the non-divergent condition of the ZMP trajectory based on the optimal control for non-divergent CoM. In Section 3.3 the three strategies for maintaining the robot balance will be carried out and we will explain how these three strategies affect the robot.

#### 3.1. Optimal Control based on Linear Inverted Pendulum Mode

The Linear Inverted Pendulum Mode (LIPM) proposed by Kajita (Kajita et al., 2001) is widely used for humanoid robot walking (Sugihara, 2009; Graf & Röfer, 2012; Santacruz & Nakamura, 2013). It simplifies the dynamics of the robot by assuming that the robot can be represented as a point mass that stands for the CoM of the robot. The relation between the ZMP and the CoM are given by:

$$p = x - \frac{z_h}{g} \ddot{x} \quad (3.1)$$

where  $p$  and  $x$  denote the position the ZMP and the CoM, and  $\ddot{x}$  denotes the acceleration of the CoM.  $z_h$  and  $g$  are the height of the CoM and the gravitational acceleration. Here it is assumed that the movement of the CoM is on a horizontal plane parallel to the ground, which implies that the height of the CoM is a constant value. Figure 3.1 shows an example of the LIPM.



### 3.1 OPTIMAL CONTROL BASED ON LINEAR INVERTED PENDULUM MODE

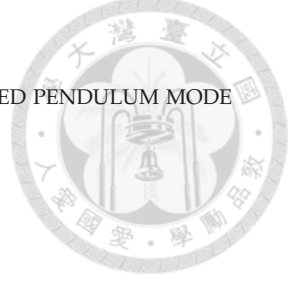
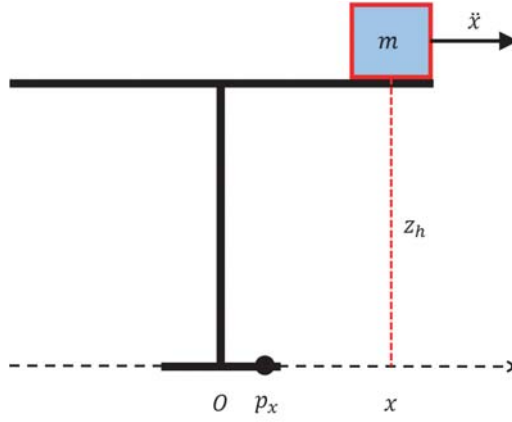


Figure 3.1. Example of the LIPM

Kajita et al. introduce the optimal control theory to the generation of the CoM Trajectory in their work (Kajita et al., 2003), which will be the foundation of this work. Here the control input  $u$  is defined as the time derivative of the  $p$ , and the equation is translated into a dynamic system as follows:

$$u = \frac{d}{dt}p$$

$$\frac{d}{dt} \begin{bmatrix} x \\ \dot{x} \\ p \end{bmatrix} = A_0 \begin{bmatrix} x \\ \dot{x} \\ p \end{bmatrix} + B_0 u \quad (3.2)$$

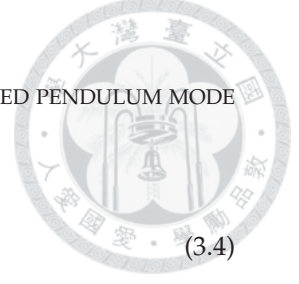
$$p = \begin{bmatrix} 0 & 0 & 1 \end{bmatrix} \begin{bmatrix} x \\ \dot{x} \\ p \end{bmatrix}$$

$$A_0 = \begin{bmatrix} 0 & 1 & 0 \\ \frac{g}{z_h} & 0 & -\frac{g}{z_h} \\ 0 & 0 & 0 \end{bmatrix} \quad (3.3)$$

$$B_0 = \begin{bmatrix} 0 \\ 0 \\ 1 \end{bmatrix}$$

After we discretize the dynamic system (3.2) with the sampling time  $\Delta t$ , the system will be

### 3.1 OPTIMAL CONTROL BASED ON LINEAR INVERTED PENDULUM MODE



$$\begin{aligned}\mathbf{x}(k+1) &= A\mathbf{x}(k) + Bu(k) \\ p(k) &= C\mathbf{x}(k)\end{aligned}\quad (3.4)$$

$$\begin{aligned}a_0 &= \Delta t + \frac{g}{3!z_h}\Delta t^3 + \frac{g^2}{5!z_h^2}\Delta t^5 + \dots \\ a_1 &= \frac{g}{2!z_h}\Delta t^2 + \frac{g^2}{4!z_h^2}\Delta t^4 + \dots\end{aligned}\quad (3.5)$$

$$\begin{aligned}A &= I_{3 \times 3} + A_0\Delta t + \frac{1}{2!}A_0^2\Delta t^2 + \frac{1}{3!}A_0^3\Delta t^3 + \dots \\ &= \begin{bmatrix} 1+a_1 & a_0 & -a_1 \\ \frac{g}{z_h}a_0 & 1+a_1 & -\frac{g}{z_h}a_0 \\ 0 & 0 & 1 \end{bmatrix} \\ B &= B_0\Delta t + \frac{1}{2!}A_0B_0\Delta t^2 + \frac{1}{3!}A_0^2B_0\Delta t^3 + \dots \\ &= \begin{bmatrix} -a_0 \\ -a_1 \\ 1 \end{bmatrix} \\ C &= [0 \quad 0 \quad 1]\end{aligned}\quad (3.6)$$

where  $\mathbf{x}(k) = (x(k), \dot{x}(k), p(k))^T$  is the state vector of the system.

Given the reference ZMP trajectory, the output ZMP is expected to be close to the reference ZMP trajectory. Meanwhile, the control input should be as low as possible. Therefore, a performance index  $J_1$  is defined as

$$J_1 = \sum_{i=k}^{\infty} \{Q_e[p(i) - p^{ref}(i)]^2 + Ru^2(i)\} \quad (3.7)$$

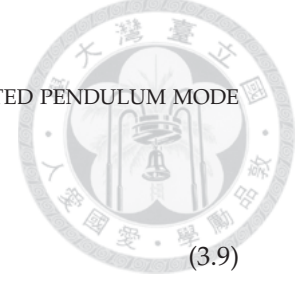
where  $Q_e$  and  $R$  are the losses due to the tracking error and the control input.

When the reference ZMP trajectory can be previewed for  $N_L$  future sampling frames, the control input (Katayama et al., 1985) that minimizes the performance index  $J_1$  is

$$u(k) = -G_x\mathbf{x}(k) + \sum_{i=1}^{N_L} G_d(i) \cdot p^{ref}(k+i) \quad (3.8)$$

where  $G_x$  and  $G_d$  are the state gain and the preview gain calculated from the weights  $Q_e$  and  $R$ , and  $K$  is the solution of the algebraic Riccati equation

### 3.1 OPTIMAL CONTROL BASED ON LINEAR INVERTED PENDULUM MODE



$$G_x = (R + B^T KB)^{-1} B^T KA$$

$$G_d(i) = (R + B^T KB)^{-1} B^T \left[ (A - BK)^T \right]^{i-1} C^T Q_e \quad (3.9)$$

$$K = A^T KA - A^T KB(R + B^T KB)^{-1} B^T KA + C^T Q_e C \quad (3.10)$$

In order to select a proper value of  $N_L$  in Eq. (3.8), we need to analyze the relation between the future sampling frames and the preview gain. Since the values of  $G_d$  cannot be observed directly, we draw all the values along the preview time to see the property of  $G_d$ . Figure 3.2 shows the relation between the preview time and  $G_d$ . We can see that the preview gain  $G_d$  approaches to zero dramatically as the preview sampling frame increases, and  $G_d$  is approximate to 0 when the preview sampling frame is at time 2 seconds. Therefore, we only preview 2 seconds ahead. In addition, in the real situation the environment changes continuously, and it is important to keep the movement of the robot flexible. Thus, only 1 step command ahead is queued, and the rest of the future step command is generated by repeating the same velocity as the current velocity. Finally, since the equation of the ZMP and the CoM in the lateral plane is the same as in the sagittal plane, the control in the both planes can be generated by Eq. (3.8).

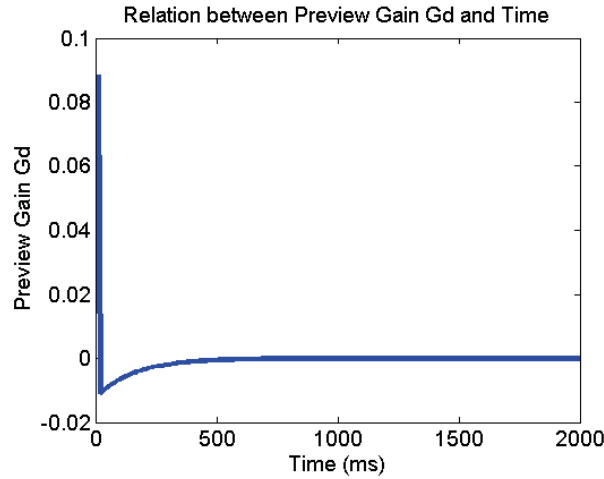


Figure 3.2. Preview Gain  $G_d$  ( $\Delta t = 10 \text{ ms}$ ,  $z = 255 \text{ mm}$ ,  $Q_e = 1$ ,  $R = 10^{-10}$ )



### 3.2. Non-divergent Condition

Researchers have found that the adjustment of the future ZMP trajectory can affect the robot balance. By combining Eq. (3.6) and Eq. (3.8), the output ZMP  $p(k+1)$  at time  $k+1$  is

$$\begin{aligned}
 p(k+1) &= C\mathbf{x}(k+1) \\
 &= CA\mathbf{x}(k) + CBu(k) \\
 &= CA\mathbf{x}(k) + CB(-G_x\mathbf{x}(k) + \sum_{i=1}^{N_L} G_d(i) \cdot p^{ref}(k+i)) \\
 &= C(A - BG_x)\mathbf{x}(k) + CB \cdot \sum_{i=1}^{N_L} G_d(i) \cdot p^{ref}(k+i)
 \end{aligned} \tag{3.11}$$

We can see that the output ZMP  $p(k+1)$  is composed of the current state  $\mathbf{x}(k)$  and the future ZMP trajectory  $p^{ref}(k+i)$ . However, whether the CoM diverges with the given future ZMP trajectory should be considered. Urata et al. (Urata et al., 2011) argue that in the optimal control the output ZMP must track the reference ZMP inside the support polygon to prevent the robot from falling down, and the control input, which is the velocity of the ZMP, does not always have severe restrictions. Therefore, they proved that if  $Q_e \gg R$ , the maximum tracking error at time  $k$  occurs at time  $k+1$ , and if the tracking error is zero at time  $k+1$ , there will be no tracking error in the whole preview time. Since the tracking error is defined as  $p(k) - p^{ref}(k)$ , to eliminate the whole tracking error, it is assumed that  $p(k+1) - p^{ref}(k+1) = 0$ , which means that the tracking error at time  $k+1$  is zero. According to the derivation above, this implies that  $p(k+i) - p^{ref}(k+i) = 0$  for all  $i > 0$ , which means that  $p(k+i) = p^{ref}(k+i)$  for all  $i > 0$ . They called this the non-divergent condition of ZMP trajectory. Given Eq. (3.11), the non-divergent condition is derived as

$$p^{ref}(k+1) = p(k+1) = C(A - BG_x)\mathbf{x}(k) + CB \cdot \sum_{i=1}^{N_L} G_d(i) \cdot p^{ref}(k+i) \tag{3.12}$$

For the sake of simplicity, we define the preview gain  $G_r(i)$  as follows:

$$G_r(i) = \begin{cases} CBG_d(1) - 1 & \text{if } i = 1 \\ CBG_d(i) & \text{if } i \geq 1 \end{cases} \tag{3.13}$$



By combining Eq. (3.12) and Eq. (3.13), we obtain the non-divergent condition:

$$C(A - BG_x)\mathbf{x}(k) + \sum_{i=1}^{N_L} G_r(i) \cdot p^{ref}(k+i) = 0 \quad (3.14)$$

Therefore, once the trajectory satisfies the non-divergent condition, the output ZMP will be equal to the reference ZMP in the whole preview time, and the robot will remain balance if and only if the reference ZMP trajectory is inside the support polygon. Figure 3.3 shows the relation between the preview time and  $G_r$ . We can see that the preview gain  $G_r$  is a negative series which approaches to zero dramatically as the preview sampling frame increases and the minimum value appears at  $G_r(1)$ .

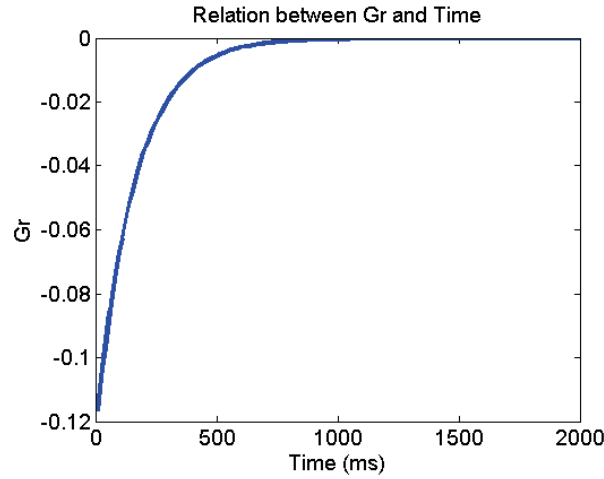


Figure 3.3. Preview Gain  $G_r$  ( $\Delta t = 10 \text{ ms}$ ,  $z = 255 \text{ mm}$ ,  $Q_e = 1$ ,  $R = 10^{-10}$ )

The advantage of the non-divergent condition is that first, since in optimal control one of the main objective is to minimize the tracking error, the non-divergent condition can provide a constraint that there is no tracking error in the whole preview time, which is the original expectation of the optimal control. Second, in the real environment the disturbance occurs in anytime, the tracking error will be accumulated and may cause the robot fall down in the future. Therefore, it is desirable that the tracking error can be compensated in every timestamp.



### 3.3. Three Strategies for Maintaining Robot Balance

Nishiwaki and Kagami proposed a three-strategy-based approach by adjusting the reference ZMP trajectory to maintain the robot balance (Nishiwaki & Kagami, 2010). In their work, the reference ZMP trajectory is modified to compensate the disturbance by considering three strategies as follows:

1. Adjusting the reference ZMP inside the sole during a step.
2. Adjusting the current step duration.
3. Adjusting the current step size.

For the second and the third strategies, a close-form solution is provided to suppress the disturbance. Later, three strategies is combined to modify the future ZMP trajectory to maintain the robot balance. The combination can be expressed as follows:

- 1:** Consider if the generated ZMP is inside the supporting polygon. If it is true, adopt the generated ZMP and break; otherwise go to **2**.
- 2:** Adjust the current step duration if the disturbance is opposite outside of the current stepping position in the lateral plane
- 3:** Adjust the current step size

However, in their work, the correlation between the three strategies is not considered. For example, when a disturbance occurs in the sagittal plane of the robot, only the step size is adjusted to compensate the disturbance. Nevertheless, not only the step size but also the reference ZMP inside the sole and the step duration affect the output ZMP. Therefore, we believe that by considering the correlation of the three strategies, the capability of the disturbance endurance can be enhanced.



## CHAPTER 4

---

### Trajectory Optimization with Simultaneous Multi-Strategy Adjustment

**I**N this chapter, we will describe the main contribution of our work. In Section 4.1 the construction of the future ZMP trajectory will be described, and the correspondence between the ZMP trajectory and the three strategies will be analyzed. In Section 4.2 the correlation among the three strategies will be evaluated and shown that the three strategies affect each other. In Section 4.3, we will define a minimum energy cost for the robot to maintain balance and show that by considering the control input, step size and step duration of the current step, the robot can generate an optimized ZMP trajectory that has the minimum energy cost and allows the robot remain balance. Finally, in Section 4.4, our approach will be compared with the traditional approaches, and we will show that with our approach, the robot can endure more disturbance and remain balance.

#### 4.1. Correspondence between the Future ZMP Trajectory and the Three Strategies

In order to analyze the correlation among the three strategies, first we need to know the correspondence between the construction of the future ZMP trajectory and the strategies. Since the basic component of the trajectory of a humanoid robot is the foot steps, the ZMP trajectory of the robot is composed of several future steps, and for each step all the reference ZMPs should be lied inside the support polygon. Here it is assumed that all the ZMPs of the following steps after the current step are placed at the center of the support polygon, and the duration of the following steps after the current step is constant. The step size is fixed for the following steps except for the current step. To simplify the trajectory,



it is assumed that there is no double support phase in the trajectory. The trajectory  $p^{ref}(i)$  can be defined as:

$$p^{ref}(k+i) = \begin{cases} p^{ref}(k+i) & \text{if } 1 \leq i \leq s_c \\ m_c & \text{if } s_c + 1 \leq i \leq s_c + s \\ m_c + m & \text{if } s_c + s + 1 \leq i \leq s_c + 2s \\ \vdots & \vdots \end{cases} \quad (4.1)$$

where  $m$  is the step size of the following step,  $m_c$  is the step size of the current step,  $s$  is the sampling frame of the duration of the following steps, and  $s_c$  is the sampling frame of the remaining duration of the current step.

In Section 3.2, we have mentioned that the output ZMP  $p(k)$  is equal to the reference ZMP  $p^{ref}(k)$  under the non-divergence condition. Therefore, given  $CA = C$ ,  $CB = \Delta t$  in Eq. (3.6) and the non-divergence condition in Eq. (3.14), the relation between every two consecutive ZMP references is

$$\begin{aligned} p^{ref}(k+1) &= p(k+1) \\ &= C\mathbf{x}(k+1) \\ &= CA\mathbf{x}(k) + CBu(k) \\ &= p(k) + \Delta t \cdot u(k) \\ &= p^{ref}(k) + \Delta t \cdot u(k) \end{aligned} \quad (4.2)$$

By considering Eq. (4.2), Eq. (4.1) can be rewritten as

$$p^{ref}(k+i) = \begin{cases} p^{ref}(k) + \Delta t \cdot \sum_{j=0}^{i-1} u(k+j) & \text{if } 1 \leq i \leq s_c \\ m_c & \text{if } s_c + 1 \leq i \leq s_c + s \\ m_c + m & \text{if } s_c + s + 1 \leq i \leq s_c + 2s \\ \vdots & \vdots \end{cases} \quad (4.3)$$

In the three-strategy-based work, the first strategy is to adjust the ZMP reference inside the sole during a step. However, in Eq. (4.3) we can see that the adjustment of the ZMP reference is equal to the adjustment of the control input  $u$ . Therefore, in our work, the three strategies are:





1. Adjusting the control input of the current step.
2. Adjusting the current step duration.
3. Adjusting the current step size.

Given the Eq. (4.1), the correspondence between the three strategies and the construction of the future ZMP trajectory is described as follows:

- 1:  $u(k+i)$  for  $1 \leq i \leq s_c$  corresponds to the control input of the current step.
- 2:  $s_c$  corresponds to the current step duration
- 3:  $m_c$  corresponds to the current step size

#### 4.2. Correlation among the Three Strategies

In the previous section, the correspondence between the three strategies and the construction of the future ZMP trajectory is demonstrated. However, how the three strategies affect each other is unknown. Therefore, now we want to show the correlation among the three strategies. We define  $p^{ref'}$  as the modified future ZMP trajectory, and  $u'$ ,  $m'_c$  and  $s'_c$  as the control input, the step size and the step duration after the adjustment. In addition, we define  $\Delta u(k+i)$ ,  $\Delta m_c$  and  $\Delta s_c$  as

$$\begin{aligned}\Delta u(k+i) &= u'(k+i) - u(k+i) \\ \Delta m_c &= m'_c - m_c \\ \Delta s_c &= s'_c - s_c\end{aligned}\tag{4.4}$$

First we analyze the correlation between the control input and the step size. Given Eq. (4.3), the future ZMP trajectory after the adjustment of the control input  $u(k+i)$  and the step size  $m_c$  should be

$$\begin{aligned}C(A - BG_x)\mathbf{x}(k) + \sum_{j=1}^{N_L} G_r(j)p^{ref'}(k+j) \\ = C(A - BG_x)\mathbf{x}(k) + \sum_{j=1}^{N_L} G_r(j)p^{ref}(k+j) + \Delta t \cdot \Delta u(k+i) \cdot \sum_{j=i}^{s_c} G_r(j) + \Delta m_c \cdot \sum_{j=s_c+1}^{N_L} G_r(j)\end{aligned}\tag{4.5}$$

Since both the original and the modified future ZMP trajectories should satisfy the non-divergent condition, by combining Eq. (3.14) and Eq. (4.5) the correlation between the control input and the step size is



$$\Delta t \cdot \Delta u(k+i) \cdot \sum_{j=i}^{s_c} G_r(j) = -\Delta m_c \cdot \sum_{j=s_c+1}^{N_L} G_r(j) \quad (4.6)$$

Figure 4.1 shows an example of the correlation between the control input and the step size. We can see that the increase of  $m'_c$  stands for the decrease of  $u'(k+i)$  and vice versa, and it is summarized that the correlation between the control input and the step size is negative.

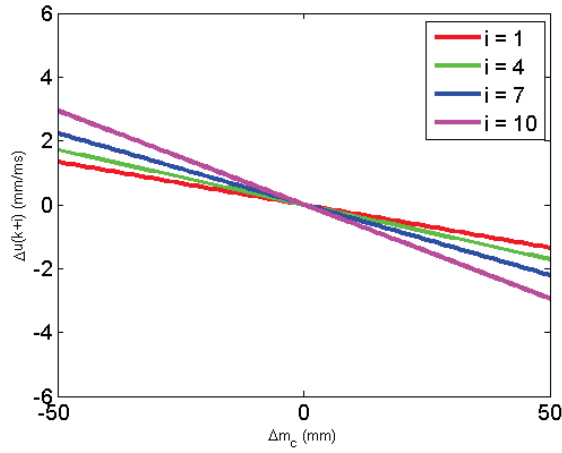


Figure 4.1. Correlation between  $\Delta u(k+i)$  and  $\Delta m_c$  ( $\Delta t = 10$  ms,  $s_c = 25 \Delta t$ ,  $N_L = 200$ )

Next we analyze the correlation between the control input and the step duration. Similar to the analysis between the control input and the step size, the future ZMP trajectory after the adjustment of the control input  $u(k+i)$  and the step duration  $s_c$  is

$$\begin{aligned} & C(A - BG_x)\mathbf{x}(k) + \sum_{j=1}^{N_L} G_r(j)p^{ref}(k+j) \\ &= C(A - BG_x)\mathbf{x}(k) + \sum_{j=1}^{N_L} G_r(j)p^{ref}(k+j) + \\ & \begin{cases} \Delta t \cdot \Delta u(k+i) \cdot \sum_{j=i}^{s'_c} G_r(j) - m_c \cdot \sum_{j=s'_c+1}^{s_c} G_r(j) & \text{if } s'_c < s_c \\ \Delta t \cdot \Delta u(k+i) \cdot \sum_{j=i}^{s_c} G_r(j) - m_c \cdot \sum_{j=s_c+1}^{s'_c} G_r(j) & \text{if } s_c < s'_c \end{cases} \quad (4.7) \end{aligned}$$



By applying the non-divergent condition, the correlation between the control input and the step duration is

$$\begin{cases} \Delta t \cdot \Delta u(k+i) \cdot \sum_{j=i}^{s'_c} G_r(j) = m_c \cdot \sum_{j=s'_c+1}^{s_c} G_r(j) & \text{if } s'_c < s_c \\ \Delta t \cdot \Delta u(k+i) \cdot \sum_{j=i}^{s_c} G_r(j) = m_c \cdot \sum_{j=s_c+1}^{s'_c} G_r(j) & \text{if } s_c < s'_c \end{cases} \quad (4.8)$$

Figure 4.2 shows the correlation between the control input and the step duration. We can see that when the sign of  $\Delta s_c$  and  $m_c$  is the same, the correlation between the control input and the step duration is negative. In contrast, if the sign of  $\Delta s_c$  and  $m_c$  is opposite, the correlation is positive.

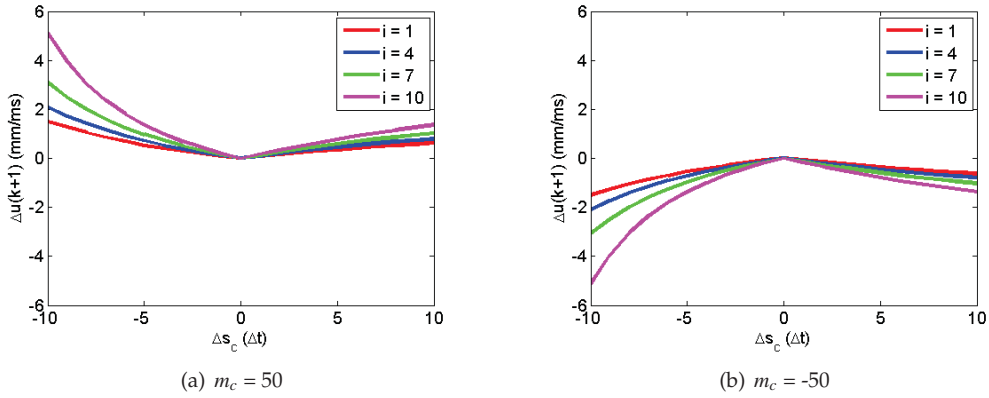


Figure 4.2. Correlation between  $\Delta u(k+i)$  and  $\Delta s_c$  ( $\Delta t = 10$  ms,  $s_c = 25 \Delta t$ ,  $N_L = 200$ )

Finally, we analyze the correlation between the step size and the step duration. The future ZMP trajectory after the adjustment of the step size  $m_c$  and the step duration  $s_c$  is



$$\begin{aligned}
& C(A - BG_x)\mathbf{x}(k) + \sum_{j=1}^{N_L} G_r(j)p^{ref'}(k+j) \\
& = C(A - BG_x)\mathbf{x}(k) + \sum_{j=1}^{N_L} G_r(j)p^{ref}(k+j) + \\
& \quad \begin{cases} \Delta m_c \cdot \sum_{j=s_c+1}^{N_L} G_r(j) + m'_c \cdot \sum_{j=s'_c+1}^{s_c} G_r(j) & \text{if } s'_c < s_c \\ \Delta m_c \cdot \sum_{j=s_c+1}^{N_L} G_r(j) - m'_c \cdot \sum_{j=s_c+1}^{s'_c} G_r(j) & \text{if } s_c < s'_c \end{cases} \quad (4.9)
\end{aligned}$$

After applying the non-divergent condition, the correlation between the step size and the step duration is

$$\begin{cases} \Delta m_c \cdot \sum_{j=s_c+1}^{N_L} G_r(j) = -m'_c \cdot \sum_{j=s'_c+1}^{s_c} G_r(j) & \text{if } s'_c < s_c \\ \Delta m_c \cdot \sum_{j=s_c+1}^{N_L} G_r(j) = m'_c \cdot \sum_{j=s_c+1}^{s'_c} G_r(j) & \text{if } s_c < s'_c \end{cases} \quad (4.10)$$

Figure 4.3 shows the correlation between the step size and the step duration. We can see that when the sign of  $m_c$  is positive, the correlation between the step size and the step duration is positive. In contrast, if the sign of  $m_c$  is negative, the correlation is negative.

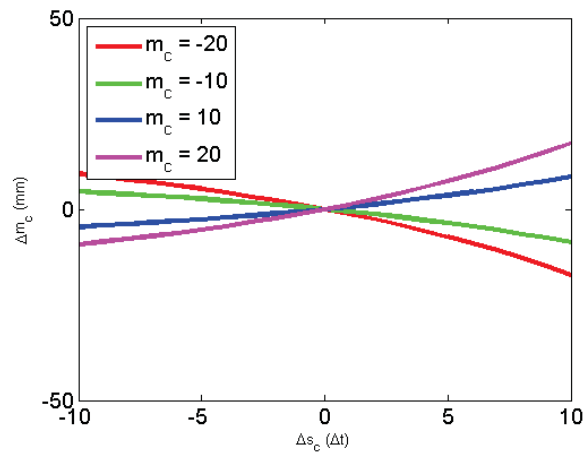


Figure 4.3. Correlation between  $\Delta m_c$  and  $\Delta s_c$  ( $\Delta t = 10$  ms,  $s_c = 25 \Delta t$ ,  $N_L = 200$ )



Figure 4.4 shows the correlation among the three strategies. It is shown that the three strategies are not independent and will affect each other.

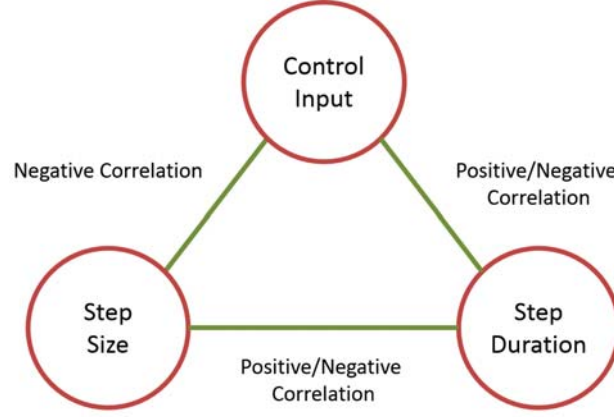


Figure 4.4. Correlation among the Three Strategies

### 4.3. Trajectory Optimization with Simultaneous Multi-Strategy Adjustment

In Section 3.3 how the strategies affect the future ZMP trajectory has been described and in Section 4.2 we have identified the correlation among the three strategies. Therefore, now the question would be: Given the current state and the future steps, how can we find a proper trajectory by applying the three strategies simultaneously?

According to the LIPM theory, without the control input, the movement of the CoM is only driven by the gravity. Thus, the control input stands for the additional energy consumption. In addition, in humanoid walking, the modification of the preplanned foot placement is often undesirable since the modified foot placement may cause the swinging foot collide with other obstacles. Therefore, the distance of the modification of the foot placement should be as small as possible. Due to the fact that the optimization of the step duration is complex, we discretize the step duration into the integer multiple of the motion cycle. For the reason above, the energy cost  $J_2$  is defined as follows:

$$J_2(s'_c) = \alpha \sum_{i=0}^{s'_c-1} u'(k+i)^2 + \beta (m'_c - m)^2 \quad (4.11)$$

For the continuous values, the Lagrange Multiplier method is applied to solve the optimal value of  $u$  and  $m'_c$ . Later, for every discrete time sample of  $s'_c$ , an optimized  $J_2$  is



calculated. At the end, the optimal value of  $u'$ ,  $m'_c$  and  $s'_c$  that minimize  $J_2$  is selected to generate the future ZMP trajectory.

The advantage of this energy function is that first, the correlation between the control input and the step size is considered. Since in Section 4.2 we have shown that the correlation is negative, in the energy cost function, the modification of the step size can be reduced by selecting a higher value of  $\beta$ , which means that the modification of the step size can be compensated by the control input. In addition, the strategy that adjusts the step size in the three-strategy-based approach can be represented in this function by setting  $\beta = 0$ , which means that it is a subset of our problem. Second, since the optimization of the function is done for every discrete sample time, the time sample that causes the energy function generating improper ZMP trajectory, such as the ZMP outside the support polygon, can be eliminated. In the three-strategy-based approach, after adjusting the step duration, if the adjustment of the step size exceeds the limitation of the robot, the step duration cannot be redesigned. However, in our approach since there are multiple combinations of the control input, the step duration and the step size, it is more possible to find a proper combination among the three strategies.

Due to the fact that the selection of  $\alpha$  and  $\beta$  is not intuitive, we apply Monte Carlo experiment to select the proper value. Figure 4.5 shows an example of the experiment result which is based on the physical model of our robot. We can see that when the ratio of  $\alpha$  and  $\beta$  is about  $10^{-4}$ , the highest success rate is reached. Therefore, we select  $\alpha = 1$  and  $\beta = 10^{-4}$  for our robot. Since the selection of  $\alpha$  and  $\beta$  depends on the physical constraint of the robot, each robot should run its own simulation experiment to find out the proper value.

In order to minimize Eq. (4.11), first we describe the construction of the trajectory in more detail. Since we know that the future ZMP trajectory should not cause the CoM diverge, by combining Eq. (3.14) and Eq. (4.3) we can get

$$\begin{aligned}
 & C(A - BG_x)\mathbf{x}(k) + \sum_{i=1}^{N_L} G_r(i)p^{ref'}(k+i) \\
 = & C(A - BG_x)\mathbf{x}(k) + l_0 + l_1 + l_2 + l_3 + \dots \\
 = & 0
 \end{aligned} \tag{4.12}$$

where  $l_n$  is

#### 4.3 TRAJECTORY OPTIMIZATION WITH SIMULTANEOUS MULTI-STRATEGY ADJUSTMENT

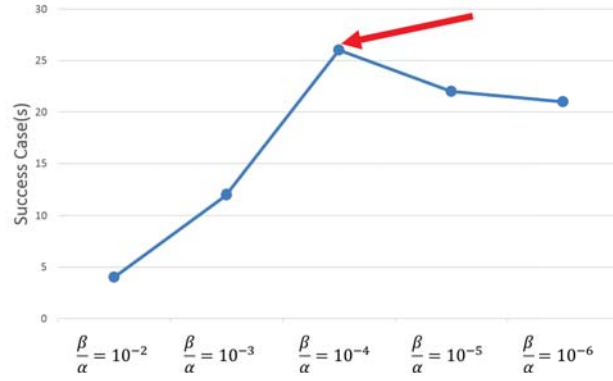


Figure 4.5. Selection of  $\alpha$  and  $\beta$

$$l_n = \begin{cases} \sum_{i=1}^{s'_c} \left( G_r(i) \cdot (p^{ref}(k) + \Delta t \cdot \sum_{j=0}^{i-1} u'(k+j)) \right) & \text{if } n = 0 \\ (m'_c + (n-1)m) \cdot \sum_{i=s'_c+(n-1)s+1}^{s'_c+ns} G_r(i) & \text{if } n \geq 1 \end{cases} \quad (4.13)$$

Eq. (4.13) can be rewritten as

$$l_n = \begin{cases} p^{ref}(k) \cdot \sum_{i=1}^{s'_c} G_r(i) + \Delta t \cdot \sum_{j=0}^{s'_c-1} \left( u'(k+j) \cdot \sum_{i=j+1}^{s'_c} G_r(i) \right) & \text{if } n = 0 \\ (m'_c + (n-1)m) \cdot \sum_{i=s'_c+(n-1)s+1}^{s'_c+ns} G_r(i) & \text{if } n \geq 1 \end{cases} \quad (4.14)$$

Since  $m$ ,  $s$ ,  $s'_c$  and  $\mathbf{x}(k)$  are known at the time when optimizing the continuous values, Eq. (4.12) and Eq. (4.14) can be rewritten as

$$\bar{c} + \Delta t \cdot \sum_{j=0}^{s'_c-1} \left( u'(k+j) \cdot \sum_{i=j+1}^{s'_c} G_r(i) \right) + m'_c \cdot \sum_{i=s'_c+1}^{N_L} G_r(i) = 0 \quad (4.15)$$

where  $\bar{c}$  is the constant value of the optimization



$$\begin{aligned}\bar{c} &= C(A - BG_x)\mathbf{x}(k) + p^{ref}(k) \cdot \sum_{i=1}^{s'_c} G_r(i) + \sum_{n=1}^{n_{max}} \hat{l}_n \\ \hat{l}_n &= (n-1)m \cdot \sum_{i=1}^s G_r(s'_c + (n-1)s + i) \\ n_{max} &= \left\lfloor \frac{N_L - s'_c}{s_c} \right\rfloor\end{aligned}\quad (4.16)$$

The Lagrange Multiplier equation that solves  $u'$  and  $m'_c$  with the given  $s'_c$  can be expressed as follows:

$$\begin{aligned}2\alpha \cdot u'(k) + \Delta t \cdot \sum_{i=1}^{s'_c} G_r(i) \cdot \lambda &= 0 \\ &\vdots \\ 2\alpha \cdot u'(k + s'_c - 1) + \Delta t \cdot \sum_{i=s'_c}^{s'_c} G_r(i) \cdot \lambda &= 0 \\ 2\beta \cdot m'_c + \sum_{i=s'_c+1}^{N_L} G_r(i) \cdot \lambda &= m \\ \Delta t \cdot \sum_{j=0}^{s'_c-1} \left( u'(k+j) \cdot \sum_{i=j+1}^{s'_c} G_r(i) \right) + \sum_{i=s'_c+1}^{N_L} G_r(i) \cdot m'_c &= -\bar{c}\end{aligned}\quad (4.17)$$

Let us define  $G_{sum}$  and  $G_{sqr}$  as

$$\begin{aligned}G_{sum}(j, k) &= \sum_{i=j}^k G_r(i) \\ G_{sqr}(j) &= \sum_{i=1}^j (G_{sum}(i, j))^2\end{aligned}\quad (4.18)$$

Therefore, the closed-form solution of  $u'$  and  $m'_c$  can be expressed as:

$$m'_c = \frac{\Delta m}{\Delta_m \lambda} \quad (4.19)$$

$$u'(k+i) = -\frac{1}{2\alpha} \cdot \Delta t \cdot G_{sum}(i+1, s'_c) \cdot \lambda \quad (4.20)$$

where





$$\lambda = \frac{\Delta\lambda}{\Delta_m\lambda}$$

$$\Delta_m\lambda = \frac{\beta \cdot G_{sqr}(s'_c) \cdot \Delta t^2}{\alpha \cdot s'_c} + (G_{sum}(s'_c + 1, N_L))^2$$

$$\Delta_m = \frac{\beta \cdot G_{sqr}(s'_c) \cdot \Delta t^2 \cdot m}{\alpha \cdot s'_c} - G_{sum}(s'_c + 1, N_L) \cdot \bar{c}$$

$$\Delta\lambda = \frac{2 \cdot \beta \cdot (m \cdot G_{sum}(s'_c + 1, N_L) + \bar{c})}{s'_c}$$
(4.21)

By selecting proper values of  $\alpha$  and  $\beta$  in Eq. (4.11), the minimum-energy ZMP trajectory can be generated by the optimal solution of  $u'$ ,  $m'_c$  and  $s'_c$ . Since  $G_r$ ,  $G_{sum}$ ,  $G_{sqr}$  can be calculated and stored before the whole process, the optimization of Eq. (4.11) can be solved in linear time.

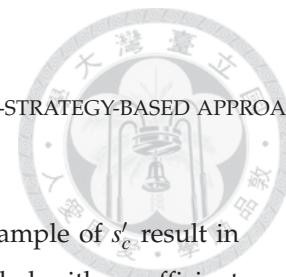
In the energy cost function, the output ZMP is not guaranteed to stay inside the support polygon. In order to know whether the robot will fall down in the future or not, we need to check if all the output ZMPs are outside the support polygon. In Section 3.2 it is shown that given the non-divergent condition, all the output ZMPs are equal to the reference ZMPs. Therefore, instead of examining all the output ZMPs, we examine the whole future trajectory, which is

$$p_l^{ref}(i) \leq p^{ref}(i) \leq p_u^{ref}(i), \quad i = 1, \dots, N_L$$
(4.22)

where  $p_l^{ref}(i)$  and  $p_u^{ref}(i)$  are the lower bound and the upper bound of the support polygon.

Since in Section 4.1 we assume that all the ZMPs of the following steps after the current step are placed at the center of the support polygon; therefore, only the ZMPs in the current step should be considered. In addition, since all the values of  $G_r$  are negative and  $G_{sum}$  is the sum of  $G_r$ , all the values of  $G_{sum}$  are also negative. Thus, all the values of  $u'(k+i)$  from Eq. (4.20) have the same sign. This implies that if the last reference ZMP of the current step is inside the support polygon, all the reference ZMP of the current step is also inside the support polygon. The last reference ZMP is composed of  $p^{ref}(k)$  and  $u'$  as

$$p^{ref}(s'_c) = p^{ref}(k) + \Delta t \cdot \sum_{i=0}^{s'_c-1} u'(k+i)$$
(4.23)



If the optimal values  $m'_c$  and  $u'$  from the current discrete time sample of  $s'_c$  result in  $p^{ref}(s'_c)$  outside of the support polygon, the energy cost  $J_2(s'_c)$  is added with a sufficient large number in order to prevent  $J_2(s'_c)$  from being selected if there exists a solution where the ZMP trajectory remains inside the support polygon. Even though our approach cannot guarantee that the output ZMP is always inside the support polygon, the solution that generates a ZMP trajectory which is inside the support polygon for the whole preview time will be selected in priority. However, if all the solutions generate a ZMP trajectory that leads to the ZMP exceeding the support polygon in the future, the  $m'_c$ ,  $u'$  and  $s'_c$  that minimize the energy cost function is still selected as the optimal solution. In this case, the robot may fall down in the future.

The main difference between our approach and the three-strategy-based approach is that in our work, the correlation among the strategies is considered through the optimization of the energy function, and the excessive adjustment caused by one strategy can be compensated by the other strategies. In addition, in the heuristic-strategy-based approach, the step duration strategy is not considered. Since in our work all the three strategies are considered, we can prevent the falling condition which can only be solved by adjusting the step duration.

#### 4.4. Comparison with the Three-strategy-based and the Heuristic-strategy-based Approaches

Since our work is based on the three-strategy-based and the heuristic-strategy-based approaches, we want to analyze the performance between ours and their works. In this section, we assume that if the robot tilts, it will fail down immediately because in their work, they do not consider the balance recovery when the robot tilts. Here we compare our work with three-strategy-based approach first. In their work, when the output ZMP exceeds the support polygon, first the ZMP is checked if it is opposite outside of the next step position in the lateral plane. If so, the step duration strategy is applied to increase the duration of the current step. Later, the step size strategy is applied in both the sagittal and lateral planes to keep the ZMP at the center of the support polygon. This may cause a problem when the disturbance is large, the step adjustment in the sagittal plane from the analytical solution may exceed the step size limit of the robot. After clipping the excessive

step size to the robot limit, the output ZMP may exceed the support polygon and the robot may fall down.

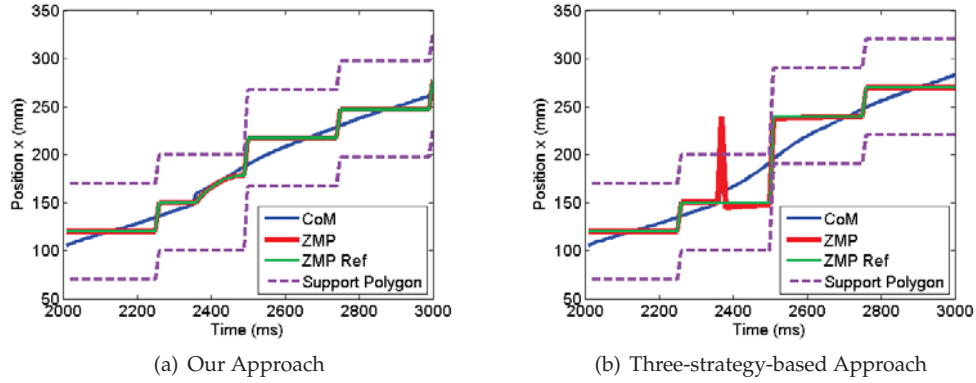


Figure 4.6. Example of Our Approach and the Three-strategy-based Approach in the Sagittal Plane

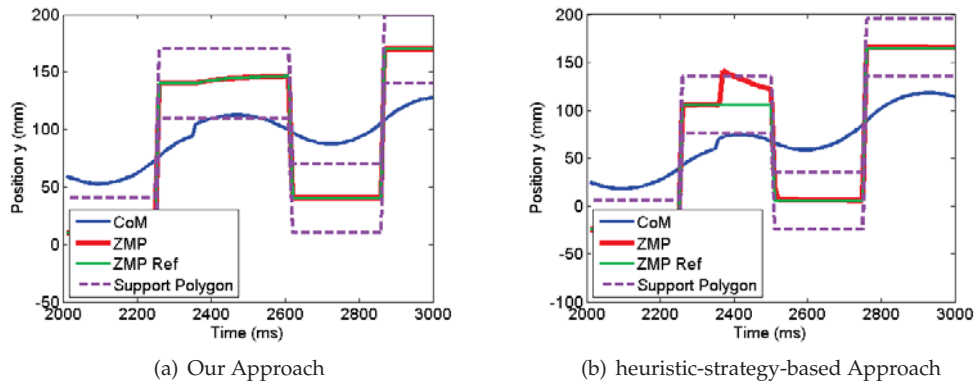
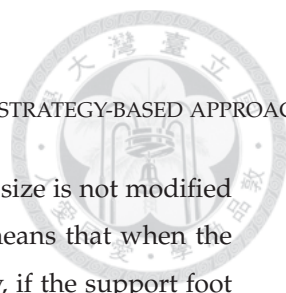


Figure 4.7. Example of Our Approach and the Heuristic-strategy-based Approach in the Lateral Plane

Figure 4.6 gives an simulation example of the difference between our work and their work. A robot with constant CoM height  $z = 255 \text{ mm}$  walking with step size  $30 \text{ mm}$  and step duration  $250 \text{ ms}$ . The step size limit of the robot in the sagittal plane is  $90 \text{ mm}$ . At time  $2360 \text{ ms}$ , a disturbance with a CoM position error  $11 \text{ mm}$  and a CoM velocity error  $0.1 \text{ mm/ms}$  occurs in the sagittal plane. We can see that with our approach the output ZMP is inside the support polygon, while with three-strategy-based approach the robot falls down.

Second we compare our work with the heuristic-strategy-based approach. In their work, only the step size is modified when the robot encounters a disturbance. However, if



the output ZMP is opposite outside of the next step position, the step size is not modified because the moving foot cannot cross its own support foot, which means that when the support foot is the left foot, the maximum step size is  $0\text{ mm}$ . Similarly, if the support foot is the right foot, the minimum step size is  $0\text{ mm}$ . Figure 4.7 gives an simulation example of the difference between our work and their work. The setting of the robot is the same as the previous example. At time  $2360\text{ ms}$ , a disturbance with a CoM position error  $10\text{ mm}$  and a CoM velocity error  $0.05\text{ mm/ms}$  occurs in the lateral plane. We can see that with our approach the output ZMP remains inside the support polygon, while with their approach the robot falls down.

Given the comparison above, we show that our approach solves the failure conditions of the three-strategy-based approach in the sagittal plane and the heuristic-strategy-based approach in the lateral plane. Therefore, with our approach, the robot can endure more disturbance in both the sagittal and lateral planes and remain balance.



## CHAPTER 5

---

### Experiment Result

**I**N this chapter the experiment results are constructed by two parts: the simulation results and the real environment results. In Section 5.1, we perform a simulation experiment with a robot that only consists of a CoM point and two massless feet, and the robot is tested with three types of disturbances. In Section 5.2, our approach is implemented in a humanoid robot Nao and is tested with different situations in the real environment. We will show that with our approach the robot can remain stable under various disturbances.

#### 5.1. Simulation Experiment

##### 5.1.1. Configuration of the Simulated Humanoid Robot

In the simulation experiment, a robot that consists of one CoM and two massless feet is simulated with a constant CoM height  $z = 255 \text{ mm}$ , and the maximum step size of the robot is  $90 \text{ mm}$  per step in the sagittal plane and  $60 \text{ mm}$  per step in the lateral plane. The support polygon of the robot is a  $100 \text{ mm} \times 60 \text{ mm}$  rectangle and the origin of the polygon is at the center of the rectangle. The robot walks with a step size  $30 \text{ mm}$  per step in the sagittal plane and  $30 \text{ mm}$  per step in the lateral plane. The step duration is  $250 \text{ ms}$  per step and the motion cycle of the robot is  $10 \text{ ms}$  per cycle. Because the robot cannot cross its leg in the lateral plane, the step size in the lateral plane is  $0 \text{ mm}$  when the support foot of the robot is its left foot. For the optimal control in the three approaches,  $N_L = 200$  is used, which means that 2 seconds of the future ZMP trajectory is considered. In our approach, we use  $\alpha = 1$  and  $\beta = 0.001$  for Eq. (4.11).



### 5.1.2. Experiment with Various Cycles of Disturbance

According to the optimal control theory, the tracking error is zero if there is no disturbance during the robot walking. Figure 5.1 shows that the ZMP is equal to the reference ZMP in both the sagittal and lateral planes when there is no disturbance.

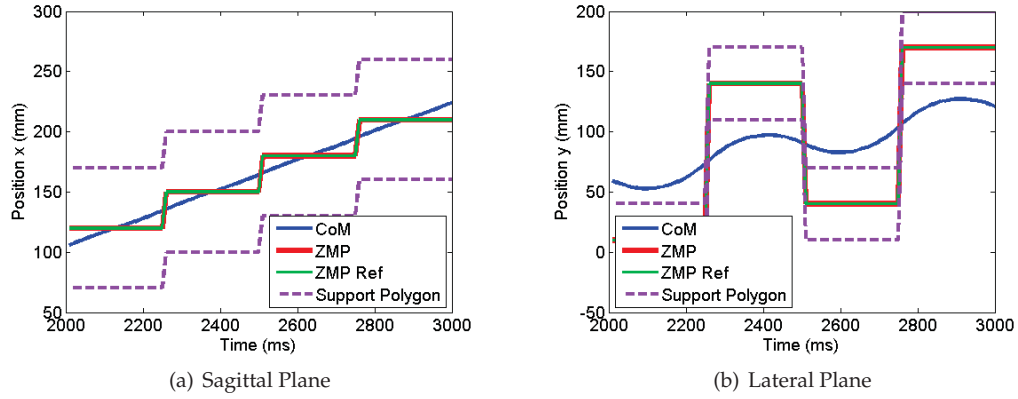


Figure 5.1. ZMP Trajectory without Disturbance

First we simulate a single-cycle disturbance at time  $2360\text{ ms}$ , where the CoM disturbance is  $2\text{ mm}$  and the ZMP disturbance is  $3\text{ mm}$  in both the sagittal and lateral planes. Since the support foot at that time is left foot, the step size in lateral plane cannot be more than  $0\text{ mm}$  due to the fact that the right foot of the robot cannot cross its left foot. In Figure 5.2, 5.3 and 5.4, we compare the reaction of the disturbance of our approach against the traditional three-strategy-based and heuristic-strategy-based approaches, and we can see that all the approaches can keep the ZMP in the support polygon, which means that the robot will not fall down when encounter such disturbance. Table 5.1 shows the detail of the three approaches after the disturbance occurs.

	Without Disturbance	Our Approach	Nishiwaki and Kagami	Urata et al.
Support Foot	Left Foot	Left Foot	Left Foot	Left Foot
Step Duration ( $ms$ )	250	260	270	250
Step Size Sagittal ( $mm$ )	30	33.4441	39.1815	37.2165
Step Size Lateral ( $mm$ )	0	-0.1167	0	0

Table 5.1. Comparison with Single-Cycle Disturbance

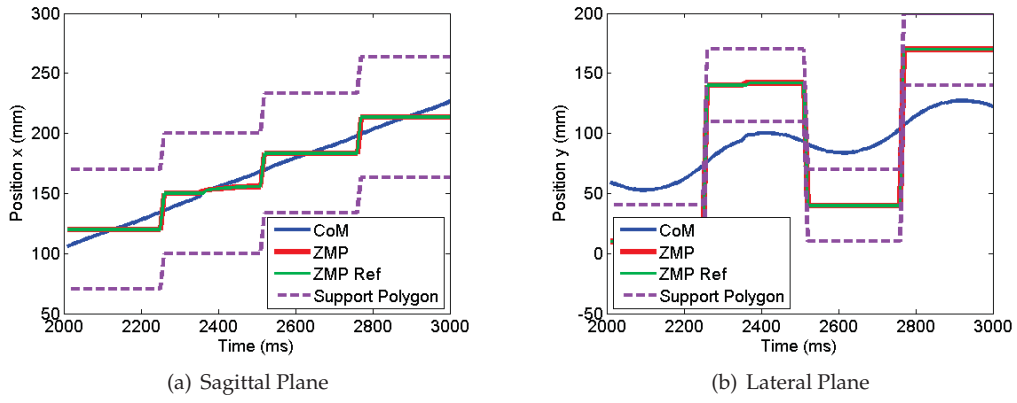
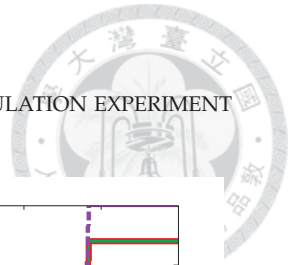


Figure 5.2. Our Approach with Single-Cycle Disturbance

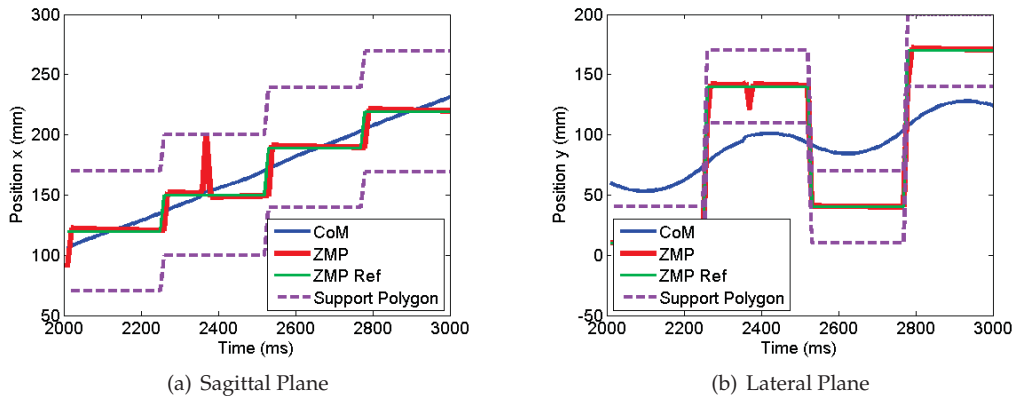


Figure 5.3. Nishiwaki and Kagami's Approach with Single-Cycle Disturbance

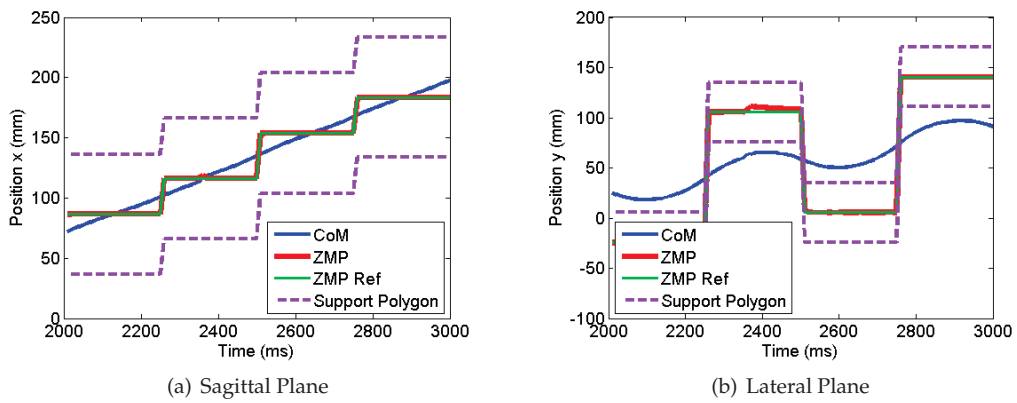


Figure 5.4. Urata et al.'s Approach with Single-Cycle Disturbance

In the real environment, the disturbance such as pushing often lasts more than one cycle. Therefore, we simulate a multiple-cycle disturbance from time 2360 *ms* to time 2440 *ms*, where the CoM disturbance is 2 *mm* and the ZMP disturbance is 3 *mm* in both the sagittal and lateral planes, which are the same as in the previous experiment. In Figure 5.5, 5.6 and 5.7, we compare the reaction of the disturbance of our approach against the traditional approaches and we find out that with our approach, the ZMP of the robot is inside the support polygon for the entire time of the disturbance and the robot remains stable. In contrast, with the traditional approaches, the ZMP is outside the support polygon and the robot will fall down. Table 5.2 shows the detail of the three approaches after the disturbance occurs.

	Without Disturbance	Our Approach	Nishiwaki and Kagami	Urata et al.
Support Foot	Left Foot	Left Foot	Left Foot	Left Foot
Step Duration ( <i>ms</i> )	250	310	430	250
Step Size Sagittal ( <i>mm</i> )	30	55.5321	90	81.3713
Step Size Lateral ( <i>mm</i> )	0	0	0	0

Table 5.2. Comparison with Multiple-Cycle Disturbance

In the three-strategy-based approach, the step duration strategy is first applied if the output ZMP is opposite outside of the next step position, and step size strategy is applied last. Since the step duration is enlarged due to the disturbance in the lateral plane, the step size in the sagittal plane should be enlarged to keep the generated ZMP inside the support polygon. Nevertheless, because the step size of the robot in the sagittal plane is limited at 90 *mm* per step, the step size strategy cannot guarantee the ZMP inside the support polygon when the generated step size from the strategy is larger than 90 *mm*. For example, in Figure 5.6, the generated step size in the sagittal plane at time 2400 *ms* is 90.1476 *mm*. After we clip the step size into 90 *mm*, the generated ZMP is 51.3778 *mm*, which is outside the support polygon and leads to the robot falling down.

In the heuristic-strategy-based approach, the step size is not modified because the step size cannot be more than 0 *mm* when the support foot is left foot. Therefore, the modification of the step size cannot keep the ZMP inside the support polygon if the output ZMP is opposite outside of the next step position. For example, we can see that in Figure 5.7, the step size in the lateral plane from 2250 *ms* to 2500 *ms* is 0 *mm* due to the limitation of the



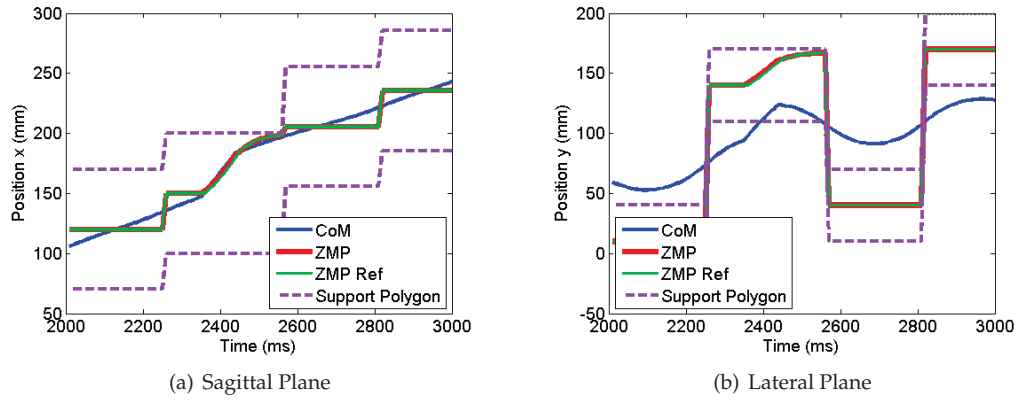


Figure 5.5. Our Approach with Multiple-Cycle Disturbance

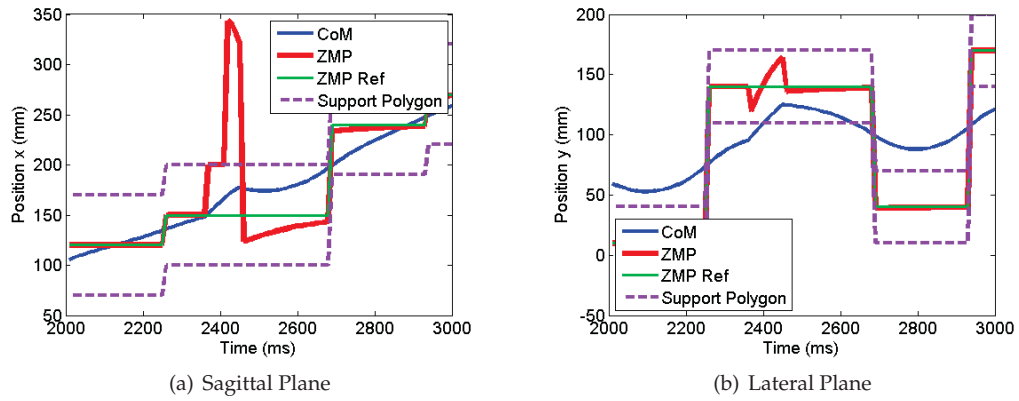


Figure 5.6. Nishiwaki and Kagami's Approach with Multiple-Cycle Disturbance

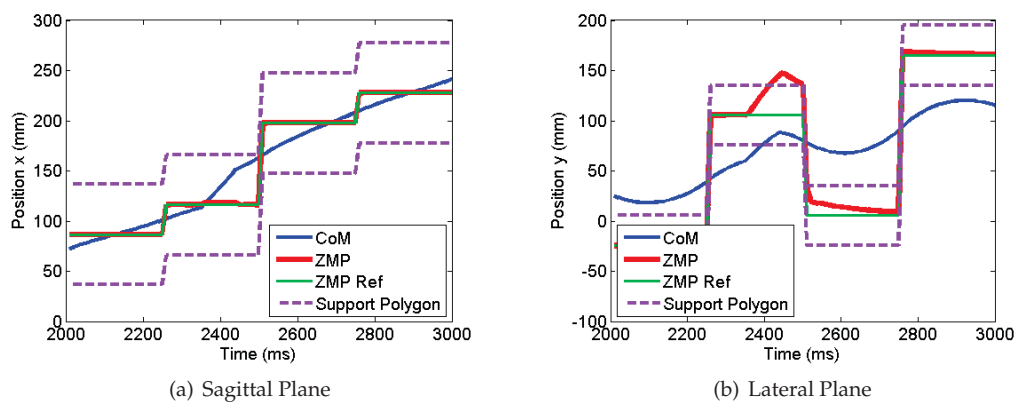


Figure 5.7. Urata et al.'s Approach with Multiple-Cycle Disturbance



robot. As the result, the ZMP is outside the support polygon and the robot fall down at time 2410 *ms*.

In addition, we want to evaluate our approach with multiple-cycle random disturbance. Here the disturbance is simulated as a multivariate gaussian distribution with zero mean value and different variance value in both the sagittal and lateral planes. There are total 5 variance values in this experiment, which are from 1 *mm* to 5 *mm* for both CoM and ZMP, and for each variance value, there are 1000 cases with the disturbance occurring for 1500 *ms*, which is about 6 step cycles of the robot. Similar to the previous simulation setting, the robot walks with a step size 30 *mm* per step in the sagittal plane and 30 *mm* per step in the lateral plane. Since the robot falls when its ZMP is outside the support polygon, we mark the case to be a success case when the ZMP remains inside the support polygon in the whole occurrence of the disturbance and mark the case to be a failure case whenever the ZMP is outside the support polygon. Table 5.3 shows the success cases of each variance and Figure 5.8 shows the result of the multiple-cycle random disturbance simulation. We can see that all of the approaches succeed when the variance is 1 *mm*. However, as the variance increases, the number of the success case of the three-strategy-based approach and the heuristic-strategy-based approach drops dramatically and our approach remains a higher number of the success case.

Variance	Our Approach	Nishiwaki and Kagami	Urata et al.
1 ( <i>mm</i> )	1000	1000	1000
2 ( <i>mm</i> )	978	692	917
3 ( <i>mm</i> )	810	71	396
4 ( <i>mm</i> )	506	1	102
5 ( <i>mm</i> )	236	0	13

Table 5.3. Comparison with Multiple-Cycle Random Disturbance

## 5.2. Real Environment Experiment

In the real environment experiment, our approach is implemented on the humanoid robot Nao, which is developed by Aldebaran Robotics Company (Gouaillier et al., 2009). The robot is 573 *mm* tall and weighs 5.2 *kg*. It has 21 degree of freedoms (DoF), 2 of which are in its neck, 4 of which are in each arm and 5 of which are in each leg. The remaining DoF is at its hip, which can control the yaw joints of both legs with only one actuated joint. Since

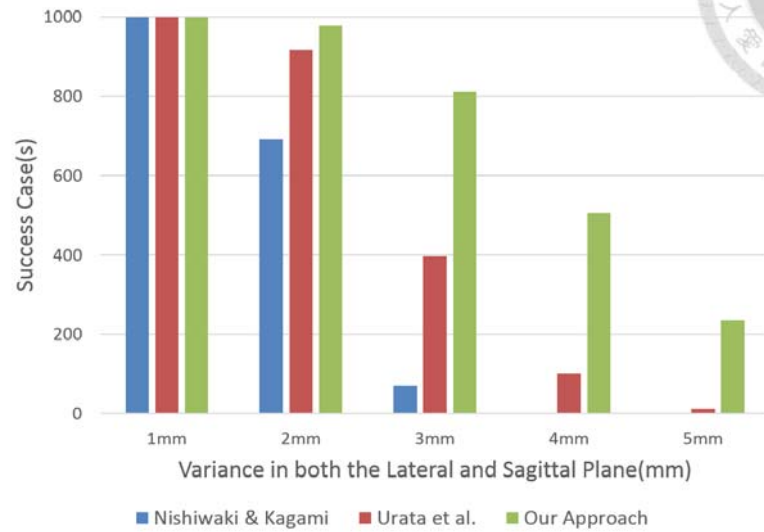


Figure 5.8. Multiple-Cycle Random Disturbance

Nao has 11 DoFs for the two legs, the inverse kinematics is more complicated than usual. Here we apply the inverse kinematics provided by Graf to overcome this issue (Graf et al., 2009). For each actuated joint, there is a magnetic rotary encoder inside to measure the position. In addition, the robot has a 3-axis accelerometer and a 2-axis gyrometer (sagittal and lateral plane) at its torso, and 4 force sensor resistors at each sole.

In this experiment, only the joint encoder is used as the feedback sensor. To acquire the current status of the CoM and the ZMP of the robot, we use Kalman Filter to estimate the state with the given dynamics of the system. In addition, the trajectory of the moving foot is based on the traditional approach (Graf et al., 2009). The height of the CoM of the robot is 255 mm and the step duration is 250 ms, which are the same as in the simulation experiment. Similarly, the motion cycle is 10 ms.

The environment setting of the experiment is similar to Alcaraz-Jimnez's work (Alcaraz-Jiménez et al., 2013) and is described as below: a stepping robot is hit by a soccer ball carried by a plastic string which is first hanged from a certain height and is released later. The soccer ball weighs 460 g and its diameter is 200 mm. For the sagittal plane, the height of the contact point is set to be 255 mm from the ground, and the ball is raised 705 mm from the ground and then is released to hit the robot. For the lateral plane, the height of the contact point is set to be 320 mm from the ground, and the ball is raised 770 mm from the

ground and then is released to hit the robot. Therefore, the potential energy of the ball in both the sagittal and lateral planes is about  $2.03 J$ . The reason why the contact points are different in two planes is that at first the disturbance is set to occur at the same height as the CoM. However, in the lateral plane, when the hand is hit by the ball, the disturbance is compensated by the hand first because there exists a space between the hand and the torso. Therefore, the height of the contact point is increased to  $320 mm$  to avoid the compensation of the disturbance from the hand. We test the balance of the robot in both the sagittal and lateral planes and see whether our approach works in both planes. For each plane, the robot receives 10 hits with our approach. In the end, the robot remains stable in all the 10 tests in both planes. Figure 5.9(a) and Figure 5.9(b) show how the environment is set in the sagittal plane and the lateral plane.

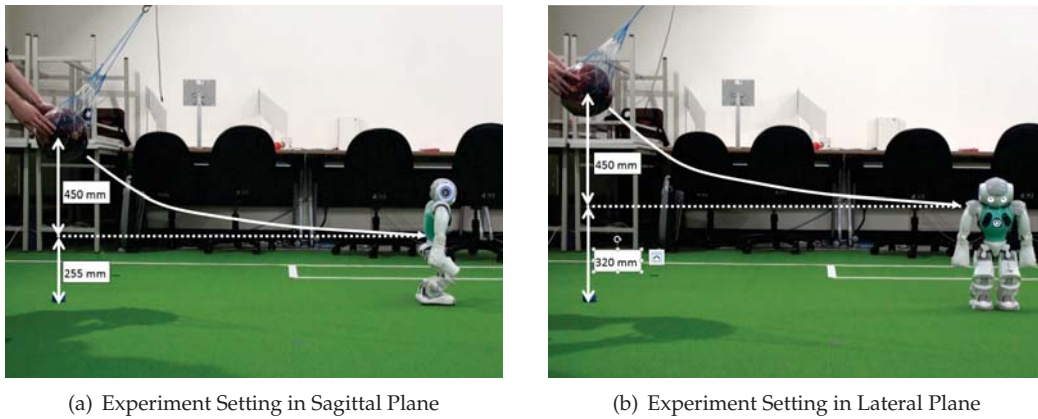


Figure 5.9. Real Environment Experiment Setting

First we discuss the result in the sagittal plane. Figure 5.10 shows one of the result of the experiment. Here the soccer ball hits the robot around time  $2700 ms$ . Before the disturbance occurs, the ZMP moves around the center of the support polygon. When the ball hits the robot, the control input and the current step size are adjusted to compensate the disturbance. Since the ball only affects the robot in the sagittal plane, the disturbance in the lateral plane is relatively small. From the figure we can see that with our approach, the ZMP remains in the support polygon in the whole experiment.

Second we discuss the result in the lateral plane. Similarly, Figure 5.11 shows one of the result of the experiment. Here the soccer ball hits the robot around time  $2900 ms$ . Since the disturbance occurs on the opposite side of the current support foot, the step size

cannot be modified and only the step duration and the control input can be adjusted to compensate the disturbance. In this experiment, the step duration is enlarged about 200 ms and the ZMP is set near to the limit of the support polygon. From the figure we can see that with our approach, the ZMP remains in the support polygon in the lateral plane.

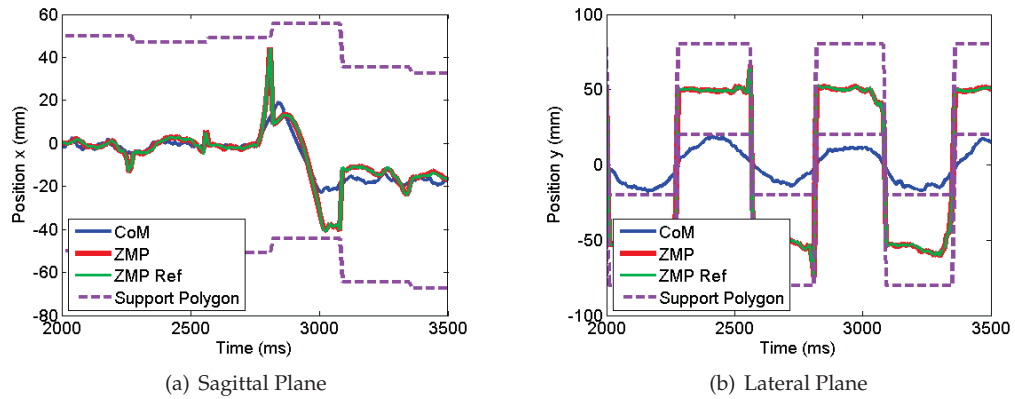


Figure 5.10. Sagittal Plane Experiment

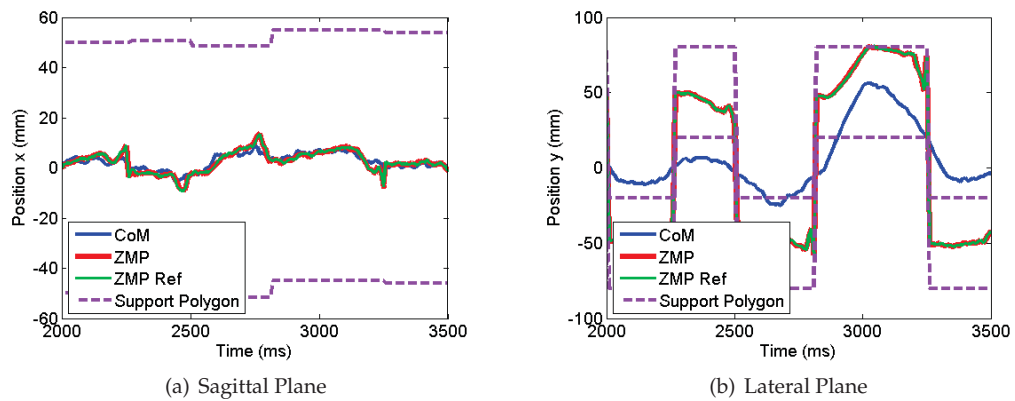


Figure 5.11. Lateral Plane Experiment



## CHAPTER 6

---

### Conclusion and Future Work

**B**ALANCE is a critical issue in humanoid robot walking. In this work, we propose the future ZMP trajectory optimization with simultaneous multi-strategy adjustment for humanoid walking balance to enhance the capacities of the disturbance compensation. First we evaluate the correspondence between future ZMP trajectory and three strategies. Next the correlation among the three strategies is analyzed. We show that the correlation exists and the three strategies affect each other. To apply the strategies simultaneously, we define an energy cost function based on the sum of the control input and the modification of the current step size. Given the non-divergent condition, the three strategies and the cost function, for every discrete sampling time, an analytical solution of the control input and the step size is solved, and the optimized step duration can be found by selecting the discrete sampling time with the least cost of the energy function. We show that with our approach, the robot can compensate more disturbances than the three-strategy-based and the heuristic-strategy-based approaches. We also implement our approach on a humanoid Nao robot and show that our approach not only works in the simulation experiment, but also enhances the stability of the robot in the real environment.

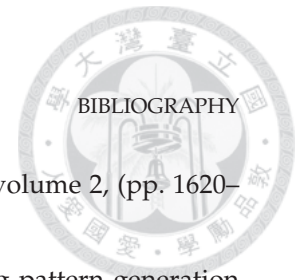
As for future work, we believe that since the uncertainties exist in the real world, we should consider the influence when the estimations of the state and the observation are uncertain. Therefore, the probabilistic approach of the state estimation, such as Kalman Filter, will be considered in the future. In addition, we would like to test our robot in more difficult scenarios, for example, pushing the robot when it is walking.



## BIBLIOGRAPHY

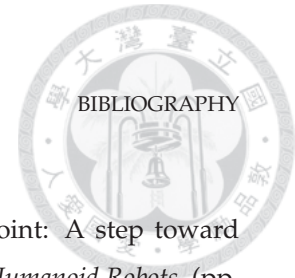
---

- Alcaraz-Jiménez, J. J., Herrero-Pérez, D., & Martínez-Barberá, H. (2013). Robust feedback control of ZMP-based gait for the humanoid robot Nao. *The International Journal of Robotics Research*, 32(9-10), 1074–1088.
- Czarnetzki, S., Kerner, S., & Urbann, O. (2009). Observer-based dynamic walking control for biped robots. *Robotics and Autonomous Systems*, 57(8), 839–845.
- Englsberger, J., Ott, C., Roa, M. A., Albu-Schaffer, A., & Hirzinger, G. (2011). Bipedal walking control based on capture point dynamics. In *IEEE/RSJ International Conference on Intelligent Robots and Systems*, (pp. 4420–4427).
- Gouaillier, D., Hugel, V., Blazevic, P., Kilner, C., Monceaux, J., Lafourcade, P., Marnier, B., Serre, J., & Maisonnier, B. (2009). Mechatronic design of NAO humanoid. In *IEEE International Conference on Robotics and Automation*, (pp. 769–774).
- Graf, C., Härtl, A., Röfer, T., & Laue, T. (2009). A robust closed-loop gait for the Standard Platform League humanoid. In *Proceedings of the Fourth Workshop on Humanoid Soccer Robots in conjunction with the 2009 IEEE-RAS International Conference on Humanoid Robots*, (pp. 30–37).
- Graf, C. & Röfer, T. (2012). A center of mass observing 3D-LIPM gait for the RoboCup Standard Platform League humanoid. In *RoboCup 2011: Robot Soccer World Cup XV* (pp. 102–113). Springer.
- Hirai, K., Hirose, M., Haikawa, Y., & Takenaka, T. (1998). The development of Honda humanoid robot. In *IEEE International Conference on Robotics and Automation*, volume 2, (pp. 1321–1326).
- Kajita, S., Kanehiro, F., Kaneko, K., Fujiwara, K., Harada, K., Yokoi, K., & Hirukawa, H. (2003). Biped walking pattern generation by using preview control of zero-moment



- point. In *IEEE International Conference on Robotics and Automation*, volume 2, (pp. 1620–1626).
- Kajita, S., Matsumoto, O., & Saigo, M. (2001). Real-time 3D walking pattern generation for a biped robot with telescopic legs. In *IEEE International Conference on Robotics and Automation*, volume 3, (pp. 2299–2306).
- Kajita, S., Morisawa, M., Harada, K., Kaneko, K., Kanehiro, F., Fujiwara, K., & Hirukawa, H. (2006). Biped walking pattern generator allowing auxiliary ZMP control. In *IEEE/RSJ International Conference on Intelligent Robots and Systems*, (pp. 2993–2999).
- Kajita, S., Morisawa, M., Miura, K., Nakaoka, S., Harada, K., Kaneko, K., Kanehiro, F., & Yokoi, K. (2010). Biped walking stabilization based on linear inverted pendulum tracking. In *IEEE/RSJ International Conference on Intelligent Robots and Systems*, (pp. 4489–4496).
- Kaneko, K., Kanehiro, F., Kajita, S., Hirukawa, H., Kawasaki, T., Hirata, M., Akachi, K., & Isozumi, T. (2004). Humanoid robot HRP-2. In *IEEE International Conference on Robotics and Automation*, volume 2, (pp. 1083–1090).
- Katayama, T., Ohki, T., Inoue, T., & Kato, T. (1985). Design of an optimal controller for a discrete-time system subject to previewable demand. *International Journal of Control*, 41(3), 677–699.
- Morisawa, M., Kanehiro, F., Kaneko, K., Kajita, S., & Yokoi, K. (2011). Reactive biped walking control for a collision of a swinging foot on uneven terrain. In *IEEE-RAS International Conference on Humanoid Robots*, (pp. 768–773).
- Morisawa, M., Kanehiro, F., Kaneko, K., Mansard, N., Sola, J., Yoshida, E., Yokoi, K., & Laumond, J.-P. (2010). Combining suppression of the disturbance and reactive stepping for recovering balance. In *IEEE/RSJ International Conference on Intelligent Robots and Systems*, (pp. 3150–3156).
- Nishiwaki, K. & Kagami, S. (2010). Strategies for adjusting the ZMP reference trajectory for maintaining balance in humanoid walking. In *IEEE International Conference on Robotics and Automation*, (pp. 4230–4236).
- Nishiwaki, K. & Kagami, S. (2011). Simultaneous planning of CoM and ZMP based on the preview control method for online walking control. In *IEEE-RAS International Conference on Humanoid Robots*, (pp. 745–751).
- Nishiwaki, K. & Kagami, S. (2012). Trajectory design and control of edge-landing walking of a humanoid for higher adaptability to rough terrain. In *IEEE/RSJ International*





- Conference on Intelligent Robots and Systems*, (pp. 3432–3439).
- Pratt, J., Carff, J., Drakunov, S., & Goswami, A. (2006). Capture Point: A step toward humanoid push recovery. In *IEEE-RAS International Conference on Humanoid Robots*, (pp. 200–207).
- Santacruz, C. & Nakamura, Y. (2013). Reactive stepping strategies for bipedal walking based on neutral point and boundary condition optimization. In *IEEE International Conference on Robotics and Automation*, (pp. 3110–3115).
- Sugihara, T. (2009). Standing stabilizability and stepping maneuver in planar bipedalism based on the best COM-ZMP regulator. In *IEEE International Conference on Robotics and Automation*, (pp. 1966–1971).
- Urata, J., Nshiwaki, K., Nakanishi, Y., Okada, K., Kagami, S., & Inaba, M. (2011). Online decision of foot placement using singular LQ preview regulation. In *IEEE-RAS International Conference on Humanoid Robots*, (pp. 13–18).
- Urata, J., Nshiwaki, K., Nakanishi, Y., Okada, K., Kagami, S., & Inaba, M. (2012). Online walking pattern generation for push recovery and minimum delay to commanded change of direction and speed. In *IEEE/RSJ International Conference on Intelligent Robots and Systems*, (pp. 3411–3416).
- Urbann, O. & Hofmann, M. (2014). Modification of Foot Placement for Balancing Using a Preview Controller Based Humanoid Walking Algorithm. In *RoboCup 2013: Robot World Cup XVII* (pp. 420–431). Springer.
- Vukobratovic, M., Frank, A., & Juricic, D. (1970). On the stability of biped locomotion. *IEEE Transactions on Biomedical Engineering*, (1), 25–36.
- Xue, F., Chen, X., Liu, J., & Nardi, D. (2012). Real time biped walking gait pattern generator for a real robot. In *RoboCup 2011: Robot Soccer World Cup XV* (pp. 210–221). Springer.



**Document Log:**

Manuscript Version 1 — 27 January 2015  
Typeset by *A.M.S.*-L<sup>A</sup>T<sub>E</sub>X — 27 January 2015

BANG-CHENG WANG

THE ROBOT PERCEPTION AND LEARNING LAB., DEPARTMENT OF COMPUTER SCIENCE AND INFORMATION ENGINEERING, NATIONAL TAIWAN UNIVERSITY, NO.1, SEC. 4, ROOSEVELT RD., DA-AN DISTRICT, TAIPEI CITY, 106, TAIWAN, *Tel.* : (+886) 2-3366-4888 EXT.407  
*E-mail address:* r02922166@ntu.edu.tw

Typeset by *A.M.S.*-L<sup>A</sup>T<sub>E</sub>X